Evaluating a Multi-jet Impingement Air Heat Exchanger Design for PEBB 6000 using Solidworks Flow Simulation

by

Qingmei Wu

Submitted to the Department of Mechanical Engineering
in partial fulfillment of the requirements for the degree of

Bachelor of Science in Mechanical Engineering

at the

MASSACHUSETTS INSTITUTE OF TECHNOLOGY

May 2020

Author .....
Department of Mechanical Engineering
May 08, 2020

Certified by .....
Thomas R. Consi
MIT Sea Grant Education Research Specialist
Thesis Supervisor

Accepted by .....
Maria Yang
Professor of Mechanical Engineering

Evaluating a Multi-jet Impingement Air Heat Exchanger Design for PEBB 6000 using Solidworks Flow Simulation

by

Qingmei Wu

Submitted to the Department of Mechanical Engineering
on May 08, 2020, in partial fulfillment of the
requirements for the degree of
Bachelor of Science in Mechanical Engineering

Abstract

The Power Electric Building Block (PEBB) 6000 is a shipboard power converter unit developed by the Navy's Electric Ship Research and Development Consortium (ESRDC). Cooling strategies for the PEBB 6000 are constrained by its size, accessibility, and high heat flux. This paper proposes an air heat exchanger design that combines a parallel plate-fin heat sink with air jet impingement onto its fins. Previous studies showed that jet impingement methods can yield heat transfer rates that are three times of those produced by conventional cooling methods, which confines a parallel flow to a surface. In order to evaluate the design feasibility of a multi-jet impingement air heat exchanger, this paper simulates the temperature contours and the flow trajectories for various multi-jet impingement models using SOLIDWORKS Flow Simulation in two stages. First, multi-jet impingement models with varying number of nozzles, nozzle diameters, impingement heights, arrangements, and velocity configurations were simulated for a single parallel plate fin. Cooler fin temperatures were achieved with larger diameter size, smaller impingement height, higher inlet velocity, and more nozzles. In the second stage, a model for the multi-jet air heat exchanger was created. When compared with simulation results for the heat sink with conventional parallel air flow, the fin thermal resistance of the heat sink was reduced by approximately 60 percent and the heat transfer rate was increased by almost threefold with the multi-jet impingement heat exchanger setup. These results help assess the potential of using a multi-jet impingement heat exchanger to cool the PEBB and provide valuable insight to improve future models.

Thesis Supervisor: Thomas R. Consi
Title: MIT Sea Grant Education Research Specialist

Acknowledgments

The author of this paper would like to express great appreciation to her research advisor and mentors at MIT Sea Grant. First and foremost, she would like to thank her advisor, Dr. Thomas R. Consi, for his immense support, patience, motivation, and enthusiasm through out her process of developing this paper and in her past undergraduate research projects. She would also like to thank Dr. Chathan M. Cooke, Dr. Chrys Chryssotomidis, and Dr. Julie Chalfant for their valuable guidance and suggestions for this paper. Special thanks to Jared David Berezin (CI instructor) for feedback on the abstract and to peers Qixin Chen, Wenzhi Li, and Cindy Chen for proofreading the thesis.

Contents

List of Figures

List of Tables

Chapter 1

Introduction

The U.S. Navy is developing all-electric naval ships as an essential step to increasing the capabilities, adaptability and affordability of the future naval forces. The Power Electric Building Block (PEBB) developed by the Navy's Electric Ship Research and Development Consortium (ESRDC) is an example of this transformation. The PEBB is a versatile power stage manager and is core to converting power from the ship's generator into an AC or DC voltage. Multiple PEBBs can be installed on a ship, depending on the required power capacity by the ship's electronic systems. Due the its power density, each PEBB unit generates enormous amounts of heat that must be rapidly removed to protect the heat-sensitive electronic components inside the PEBB.

The ESRDC recently proposed several thermal management options for the PEBB, such as using air cooling, liquid cooling, and jet impingement of two-phase dielectric materials. Due to dimensional and proximity to liquid constraints, each of the options has both advantages and disadvantages. In particular, this paper proposes the design of a two-step cooling method by combining a parallel fin heat sink and a manifold-style air heat exchanger, as illustrated in Figure 1-1. In the first step, the parallel fin heat sink adhered onto the surface of the PEBB disperses heat through its fins. A manifold with drilled channels overlays the heat sink in a parallel manner. Chilled and high pressured air is pushed through a main inlet. The air will exit each hole in the channels as air jets, resulting a multi-jet impingement on the surfaces of the parallel fins. For the rest of this paper, this cooling option is referenced as the multi-jet

impingement air heat exchanger.

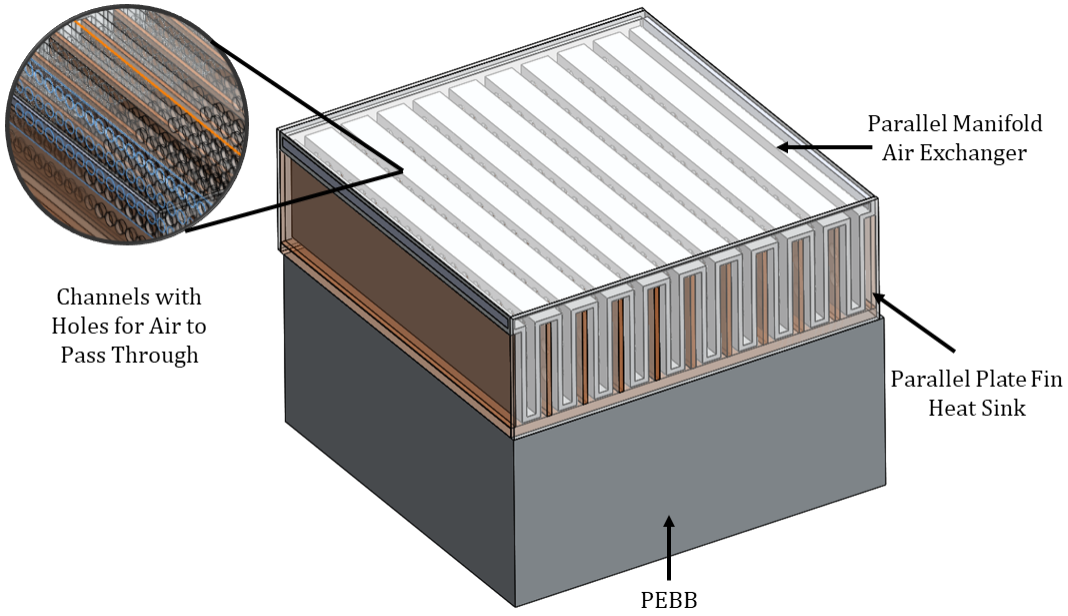

Figure 1-1: Illustration of setup for multi-jet impingement air heat exchanger

Figure 1-2 in the following page displays the ideal air flow through the heat exchanger. The purple arrows represent inflow of cold air from the main inlet and the red arrow represent the exit of warm air to the outlets. Unlike conventional forced wall-parallel flow in heat sinks, the air jets are orthogonal to the surface. Work by Zuckerman and Lior (2006) stated that jet impingement has the potential to produce heat transfers rates that are three times the heat transfer rates for conventional convection cooling confined by a parallel flow to a surface.

This paper applies the governing nondimensional parameters of jet impingement and SOLIDWORKS Flow Simulation to study and evaluate a design of the multi-jet impingement air heat exchanger. Chapter 2, Background, provides further detail regarding the PEBB and summarizes governing equations for jet impingement and conventional forced wall-parallel flow in heat sink. Chapter 3, Model, presents detailed description and diagrams for each of the models that were studied using SOLIDWORKS Flow Simulation. Chapter 4 discusses the procedure for SOLIDWORKS Flow Simulation and how the boundary conditions, initial conditions, and set goals for convergence were specified. In addition, diagrams for each model shown in Chap-

ter 3 are presented. In Chapter 5, Results, simulation results are presented for each model. Chapter 6, Conclusion and Future Works, summarizes the paper and outlines future steps to simulate the new multi-jet air heat exchanger models.

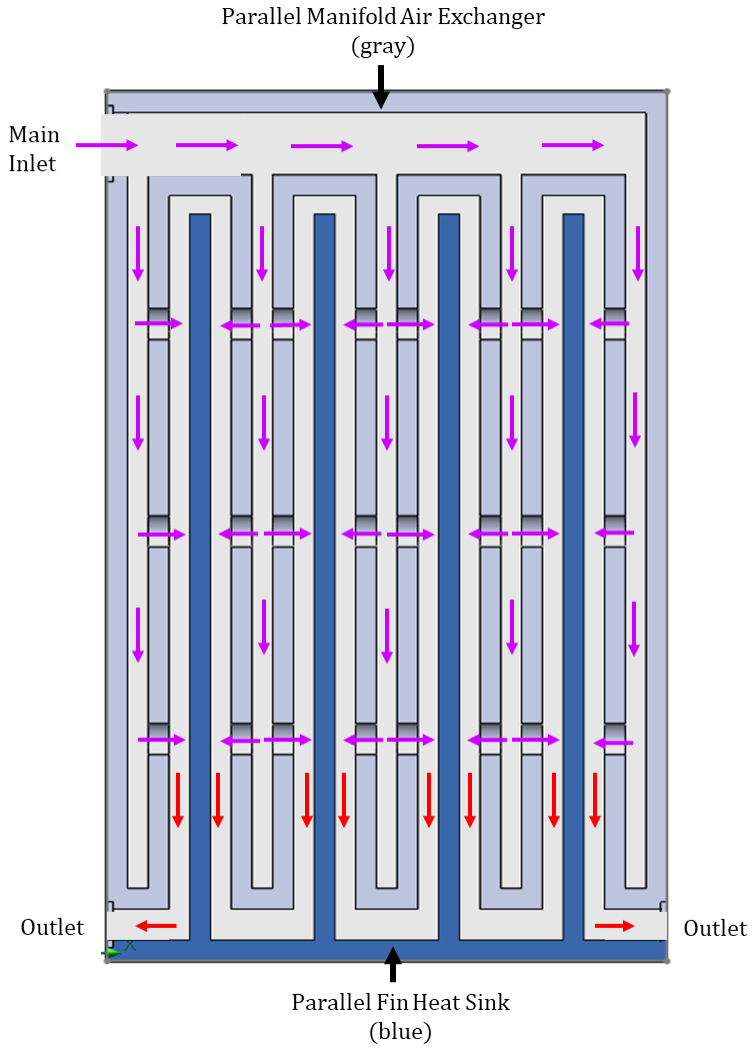

Figure 1-2: Ideal air flow in the multi-jet air heat exchanger. Purple arrows indicate flow of cold air from the main inlet and the red arrows indicate the exit of warm air through the outlets.

Chapter 2

Background

This section introduces the relevant background for this paper. Section 2.1 outlines the purpose and thermal management system requirements of the PEBB 6000. Section 2.2 summarizes the governing parameters and equations for jet impingement. Section 2.3 recaps the governing equations for conventional convective parallel flow cooling on heat sinks.

2.1 Cooling the PEBB 6000

As discussed in Chapter 1, the PEBB 6000 is a shipboard Power Electronic Building Block developed by the Navy's Electric Ship Research and Development Consortium (ESRDC) for the electronic power management system on a Navy ship. The PEBB acts as a unit power stage manager and converts power from the ship's generator into an AC or DC voltage. In the latest design update, each PEBB unit has an approximate length of 20 inches, a width of 13 inches, and a height of 10 inches [1]. The PEBB has a high heat flux of 100 W/cm^2 due to its compact and high power density [4]. One of the current challenges is to design a thermal management system that can effectively remove a thermal load of 6 kW of heat from the PEBB [4]. However, the thermal management system design is subject to two main design constraints. First, the thermal management system and the PEBB should be easily replaceable by a sailor. Second, the system should not contain or should minimize

liquid connections near the PEBB.

The ESRDC group has proposed several thermal management systems for the PEBB [5]. The first option is to apply air cooling by using a large volume of air to cool the surface of the PEBB, However, this will require a larger and heavier PEBB to have a larger heat transfer surface [1, 4]. The second option is to apply liquid cooling on the PEBB surface, but will require a reliable leak detection and protection system [4]. In the third option, external liquid cools a dry interface connected to the PEBB [4]. This option relies heavily on the thermal resistance at the contact between the dry interface and the PEBB. The fourth option suggests jet impinging two-phase dielectric material onto the PEBB surface, but will require an additional layout to remove the dielectric material [4]. The fifth option is the multi-jet air heat exchanger proposed in this paper. The multi-jet air heat exchanger is a two-step cooling method that combines a parallel fin heat sink and a manifold-style air heat exchanger. For a more specific description of this option, please refer to Chapter 1.

2.2 Jet Impingement

Jet impingement can be implemented by releasing a directed jet of liquid or gaseous flow against a surface to enhance heat transfer. Applications of this method can be seen in electronic cooling, optical surface heating, and material forming [6]. Section 2.2.1 discusses different jet impingement regions. Section 2.2.2 summarizes the parameters and governing equations for jet impingement that are relevant to the models discussed in Chapter 3.

2.2.1 Impinging Jet Regions

An impinging jet confined between a confinement plate and a bottom wall has five main regions: the free jet region, the impingement region, the stagnation region, the wall jet region, and the recirculation region. Figure 2-1 shows these five different regions for a single impinging jet.

To start, the jet of fluid exiting the nozzle will enter the free jet region, where

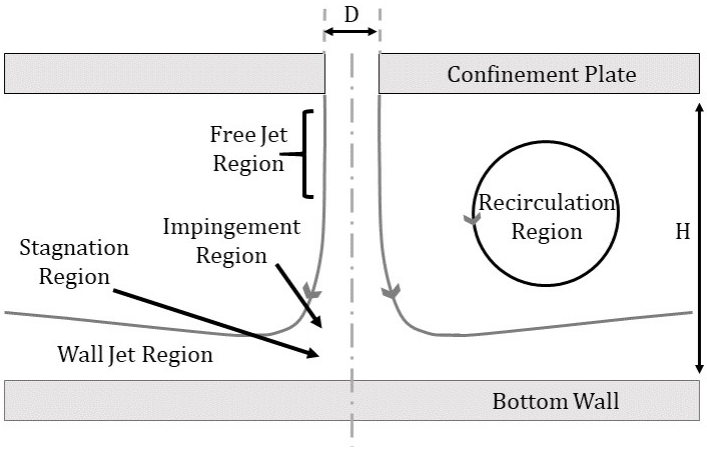

Figure 2-1: Jet Impingement Regions

it can behave as a free submerged jet. Because the free jet region is sufficiently far enough from the jet impingement surface, the jet shears at its edges and transfers its momentum laterally outward. For a free jet region to exist, the exit of nozzle and the impingement plate must be at least two nozzle diameters apart [6]. Kwon et al. (2020) also stated that heat transfer is enhanced when the ratio between nozzle length (L) and nozzle diameter (D) is greater than 4. As the jet enters the jet impingement region, its energy decays and its velocity increases due to viscous diffusion of momentum [3, 6]. The jet velocity profile becomes more Gaussian as it continues to decay in the jet impingement region [6]. When the jet arrives at the stagnation region, it decelerates and loses its axial velocity. This results in high static pressure on the impingement surface and a nonuniform turning flow. After turning, the flow enters into the recirculation region adjacent to the jet [6].

2.2.2 Jet Impingement Governing Parameters and Equations

To understand the governing parameters and equations for jet impingement, one can identify jet impingement as a system consisting of three main components: the nozzle, the jet fluid, and the impingement surface. For the purpose of this paper, a cylindrical nozzle with diameter D is chosen. The jet exiting the nozzle has an initial jet temperature T_{0jet}, velocity U_{jet}, density ρ_{jet}, and viscosity μ_{jet}. The impingement wall has a temperature at T_{wall} and is a distance of H away from the exit of the

nozzle.

The non-dimensional ratio formed using the Nusselt number and the Sherwood number is frequently used to categorize heat transfer and mass transfer of impinging air jets [6].The definition of the Nusselt number is $Nu = hD_h/k_c$, where h is the heat transfer coefficient, D_h is the hydraulic diameter, and k_c is the thermal conductivity of the fluid. Let $\partial T/\partial \overrightarrow{n}$ represent the temperature gradient normal to the impingement wall, the heat transfer coefficient for an impinging jet with a temperature gradient can be defined as equation 2.1 [6].

$$h = \frac{-k_c \partial T/\partial \overrightarrow{n}}{T_{0jet} - T_{wall}}. \tag{2.1}$$

The Sherwood number is defined as $Sh = k_i D_i/D_{diff}$, where k_i is the convective mass transfer rate, D_{diff} is the mass diffusivity, and D_i is the characteristic length. The characteristic length is the nozzle diameter for jet impingement. Let $\partial C/\partial n$ denote the mass concentration gradient component normal to the impingement wall, C_{0jet} denote the mass concentration of the jet, and c_{wall} denote the mass concentration at the impingement wall, then the convective mass transfer rate k_i can defined as equation 2.2 [6].

$$k_i = D_{diff} \frac{\partial C/\partial n}{C_{0jet} - C_{wall}}. \tag{2.2}$$

In addition to the nondimensional parameters discussed above, Table 2.1, adapted from a list in Zuckerman and Lior (2006), lists several other relevant parameters and ratios to describe an impinging jet.

Parameter	Definition
Pr	Prandtl number of the fluid
H/D	Nozzle height to nozzle diameter ratio
r/D	Nondimensional radial position from the center of the jet
Tu	Nondimensional turbulence intensity
Re_0	Reynolds number defined as $U_{jet}D/\nu_{jet}$
p_{jet}/D	jet center-to-center spacing (pitch) to diameter ratio

Table 2.1: Other Important Parameters for Jet Impingement

2.2.3 Important Design Parameters for Jet Impingement

Two of the most important design parameters for jet impingement are nozzle shape and the distance H, which is the distance between the exit of the nozzle and the impingement surface. Nozzle shape can affect the performance of jet impingement design. The nozzle where the fluid exits prior to the free jet region controls the specific temperature, velocity, and turbulence characteristics of the impinging jet. For example, a jet of fluid exiting a pipe or cylindrical-shaped nozzle will have high initial turbulence, low free jet shearing force, high pressure drop, and nearly parabolic velocity profile at the nozzle exit [6]. On the other hand, a jet of fluid exiting a nozzle with a contoured contraction will tend to have a low initial turbulence, moderate to high free jet shearing force, low pressure drop, and a uniform velocity profile [6]. The typical Reynolds number range for a gas jet is between 4,000 to 80,000 [6]. The expected H/D ratio spans from 2 to 12 [6]. The Nusselt number increases as H decreases, indicating a better heat transfer. Ideally, the smallest value of H should be chosen first and then a nozzle diameter should be selected accordingly when a designing jet impingement setup [6].

2.3 Parallel Plate Fins

Parallel plate fin heat sinks are essential for many electronic cooling applications. Section 2.3.1 first recaps the derivation of the fin equation with a convective heat transfer tip condition and then outlines the equations to evaluate fin efficiency. Section

2.3.2 summarizes the governing equations for the thermal resistance of a parallel plate fin derived using the parallel plate fin heat sink.

2.3.1 Fin with Convective Heat Transfer Tip Condition

A parallel plate fin made of a material with thermal conductivity k is submerged in air with ambient temperature T_∞. The fin uniform cross-sectional area A_c and cross sectional perimeter P are shown in Figure 2-2. To simplify the derivation of the fin equation, it is assumed that the fin's material properties are independent of temperature and convection is uniform across the fin's surface area. The following equations are adapted from the textbook *A Heat Transfer Textbook, 5^{th} edition* [2].

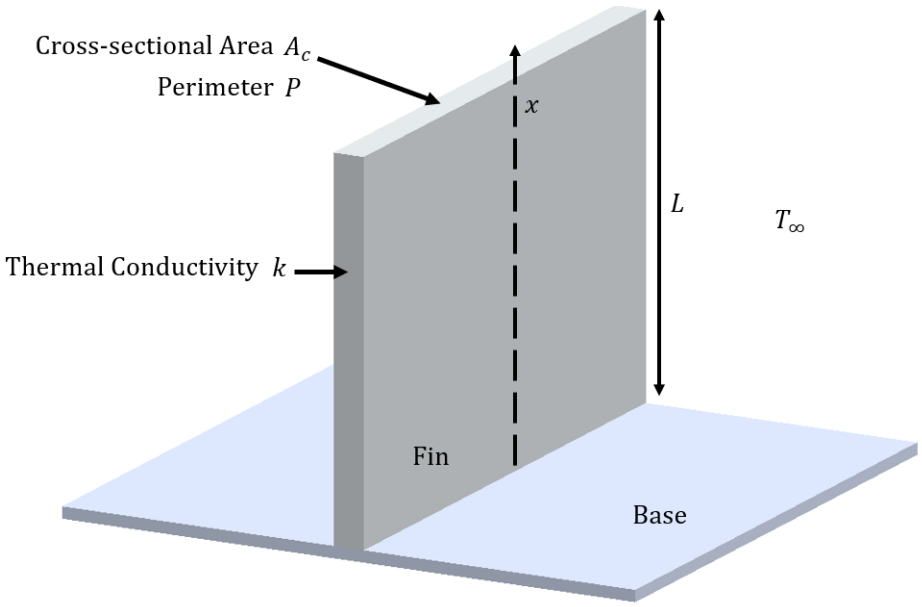

Figure 2-2: Parallel Plate Fin

By applying the conservation of energy for the heat flow rate for a differential element of the fin, the energy balance equation for one-dimensional conduction in the x-direction is:

$$\dot{Q}(x+dx) = \dot{Q}(x) + d\dot{Q}_{convection}(x). \tag{2.3}$$

Next, Fourier's law is applied to rewrite $\dot{Q}(x)$ and the flux $\ddot{q}$ as:

$$\dot{Q}(x) = -kA_c\frac{dT}{dx} \tag{2.4}$$

$$\ddot{q} = h(T - T_\infty), \tag{2.5}$$

where T is the temperature T(x) at a given position along the x-direction of the fin. Using the fin cross sectional perimeter and the fin's heat transfer h, the differential convective heat flux can be expressed as:

$$d\dot{Q}_{convection} = Ph(T - T_\infty)dx. \tag{2.6}$$

Substituting equations 2.4 and 2.6 back into the energy balance equation, the general fin governing equation is

$$-kA_c(\frac{dT}{dx})|_{x+dx} = -kA_c(\frac{dT}{dx})|_x + Ph(T - T_\infty)dx, \tag{2.7}$$

which can be simplified to:

$$k\frac{d}{dx}(A_c\frac{dT}{dx}) = Ph(T - T_\infty). \tag{2.8}$$

Because the fin has a constant cross-section across its length, the fin equation can further be simplified into:

$$\frac{d^2T}{dx^2} = \frac{hP}{kA_c}(T - T_\infty). \tag{2.9}$$

By defining $\theta(x) = T(x) - T_\infty$, $\theta_b(x) = T_b - T_\infty$, and the fin parameter m by: $m^2 = \frac{hP}{kA_c}$, then the temperature distribution profile for a fin with convective heat transfer tip condition is:

$$\frac{\theta}{\theta_b} = \frac{coshm(L - x) + (\frac{h}{mk})sinhm(L - x)}{coshmL + (\frac{h}{mk})sinhmL} \tag{2.10}$$

The performance of the fin can be evaluated using the fin efficiency and the fin effectiveness [2]. Fin efficiency is the ratio of the fin heat transfer rate $\dot{Q}_f$ to the heat transfer rate of the fin assuming the entire fin was set at the base temperature. Fin

effectiveness is the ratio of fin heat transfer rate $\dot{Q}_f$ to the heat transfer rate without a fin (for the same object). The two performance formulas are almost identical, except fin efficiency uses surface area of the fin (A_f) for calculation while fin effectiveness uses the fin cross-sectional area at the base ($A_{c,b}$). The formula for fin efficiency is:

$$\eta_f = \frac{\dot{Q}_f}{hA_f\theta_b} \tag{2.11}$$

and the formula for fin effectiveness is:

$$\varepsilon_f = \frac{\dot{Q}}{hA_{c,b}\theta_b} \tag{2.12}$$

2.3.2 Thermal Resistance of a Parallel Plate Fin Heat Sink

Figure 2-3 presents a parallel plate fin heat sink. The parallel fins on the heat sink have constant sections across its length. Each fin has length L_f, width W_f, thickness t_f, base thickness t_b, and fin base temperature T_f. A heat source $\dot{Q}$ is dissipating at the heat sink base with a temperature T_{hs}. Let R_b denote the thermal resistance of the heat sink base, R_f denote the thermal resistance of the parallel plate fin, and R_{eq} denote the total equivalent thermal resistance. Assuming the base has a cross-section area A_b, then the thermal resistance for the base is:

$$R_b = \frac{t_b}{kA_b}. \tag{2.13}$$

The thermal resistance for the fin is a function of the fin efficiency η_f, number of fins n, and the dimensions of the fin.

$$R_f = \frac{1}{nh_fW_f(t_f + 2\eta_f L_f)} \tag{2.14}$$

The total equivalent thermal resistance is:

$$R_{hs} = R_b + R_f. \tag{2.15}$$

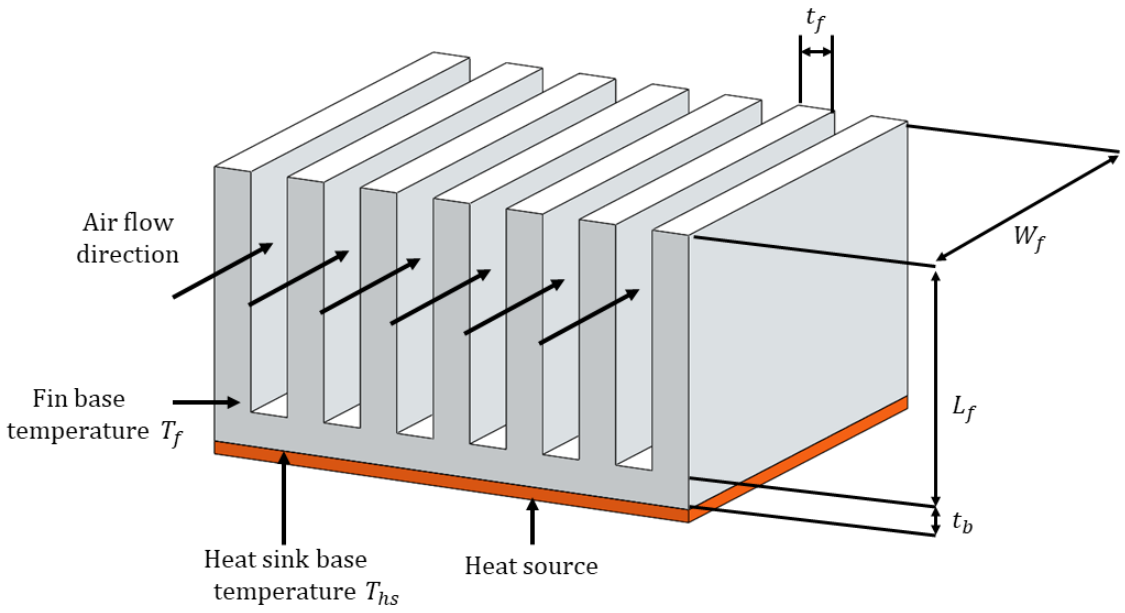

Figure 2-3: Parallel Plate Fin Heat Sink

Chapter 3

Models

The models presented in the following sections are modified from the general model for multi-jet impingement on a parallel plate fin shown in Figure 3-1. In Figure 3-1a, an aluminum parallel plate fin is enclosed in a box. The dimension of the box is 52 mm by 7 mm by 37 mm (L_{box} x W_{box} x H_{box}). Three D mm wide holes, representing cylindrical nozzles, are placed along the center line of the Y-Z plane faces of the box. These three holes are mirrored to the other side of the box to represent outlets, as shown in Figure 3-1c. The center-to-center distance between the holes is 10 mm. The parallel plate fin in Figure 3-1b has a thickness (t_f) of 1 mm, a length (L_f) of 25 mm and and a width (W_f) of 50 mm. The surface of the fin facing the nozzles is located H mm away from the exit of nozzles. The gap between the bottom surface of the fin and the bottom surface inside the box is 5 mm wide. Table 3-1 outlines the parameters described above.

Four different variations of models are tested. In Section 3.1, the nozzle diameter is varied. In Section 3.2, the distance between nozzle exit and the impingement surface is varied. In Section 3.3, three different patterns of nozzle arrangements are modeled. In Section 3.4, models with different configurations of inlet velocities are compared. In Section 3.5, the model for the whole multi-jet impingement air heat exchanger is presented.

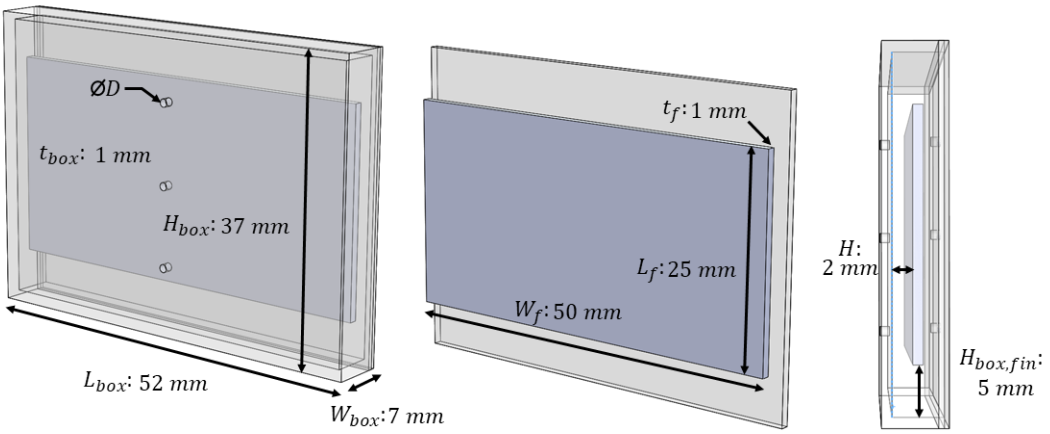

Figure 3-1: General model setup for multi-jet impingement on parallel plate fin. (a) Dimensions of the box enclosing the parallel plate fin. (b) Dimensions of the parallel plate fin. (c) Location of the fin inside the box.

Parameter	Definition	Value
t_f	Thickness of fin	1 mm
L_f	Length of fin	25 mm
W_f	Width of fin	50 mm
L_{box}	Length of box	52 mm
W_{box}	Width of box	7 mm
H_{box}	Height of box	37 mm
t_{box}	Thickness of box	1 mm
$H_{box,fin}$	Distance from bottom of fin to bottom surface of box	5 mm
S	center-to-center distance between nozzles	10 mm
D	Nozzle Diameter	Variable
H	Distance between nozzle exit and impingement wall	Variable

Table 3.1: Parameter and dimensions of general model.

3.1 Varying Nozzle Diameter

Nozzle diameter controls the initial conditions of the air jet. Three different nozzle diameters are tested by modifying the general model. Figure 3-2 displays the models for $D = 0.75$ mm, $D = 1.0$ mm and $D = 1.5$mm in sub-figures (a), (b), and (c) respectively. The center-to-center distance between the nozzles is 10 mm and the impingement height is 2 mm. The boundary and initial conditions are also constant

across all three nozzles. Specific values for the boundary and initial conditions can be found in Chapter 4.

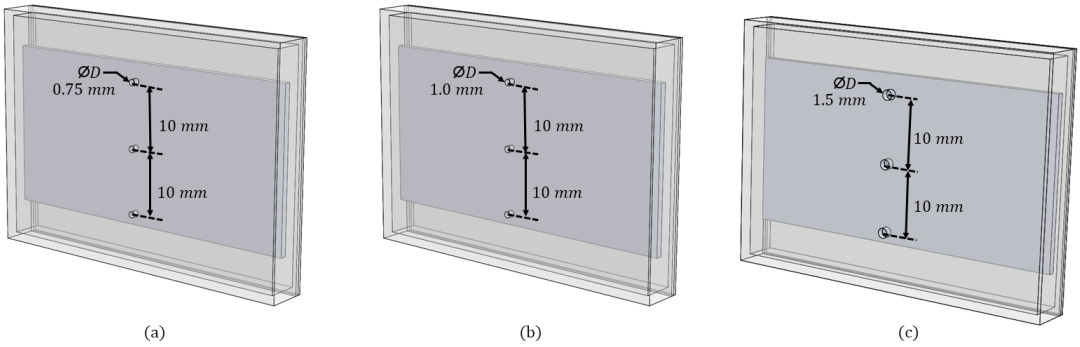

Figure 3-2: Models with varying nozzle diameters. (a) $D = 0.75$ mm. (b) $D = 1.0$ mm. (c) $D = 1.5$ mm.

3.2 Varying Impingement Height

This sets of models test how varying distance between nozzle exit and impingement surface affects the temperature of the parallel plate fin. Figure 3-3 displays the models for $H = 1.0$ mm, $H = 2.0$ mm and $H = 3.0$ mm. Like models in the last section, the center-to-center distance between nozzles is 10 mm. The nozzle diameters are set to 1.0 mm. The boundary and initial conditions are also constant across all three nozzles.

3.3 Nozzle Pattern and Arrangement

The goal of the models in this section is to visualize how the number and pattern arrangement of nozzles affect the temperature of the fin. Three different pattern configurations are shown in Figure 3-4: the general model, the cross pattern, and the square pattern. The cross pattern is the general model with two new nozzles added to the left and right of the center nozzle. The square pattern is a 3 by 3 array of nozzles. All the nozzle diameters are set to 1.5 mm. The nozzle centers are spaced 10 mm from each other horizontally and vertically.

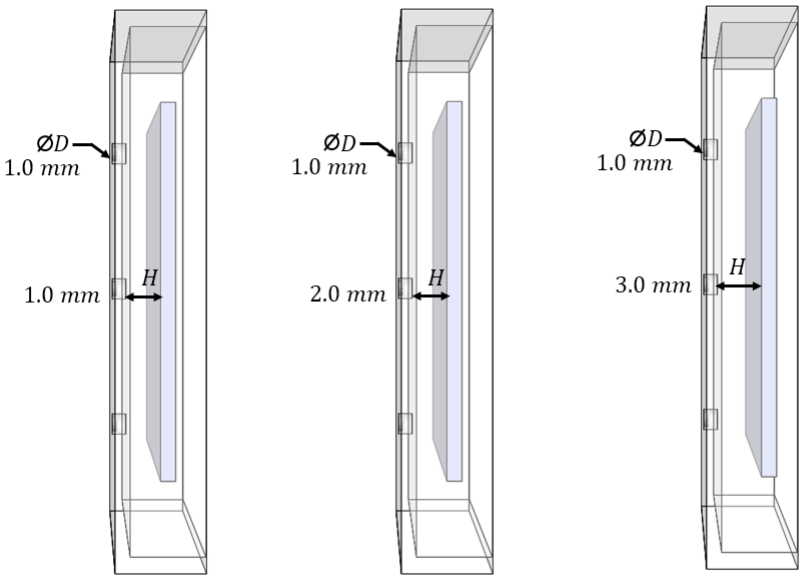

Figure 3-3: Varying distance between nozzle exit and impingement surface. The nozzle diameters are set to 1.0 mm. (a) H =1.0 mm. (b) H = 2.0 mm. (c) H = 3.0 mm.

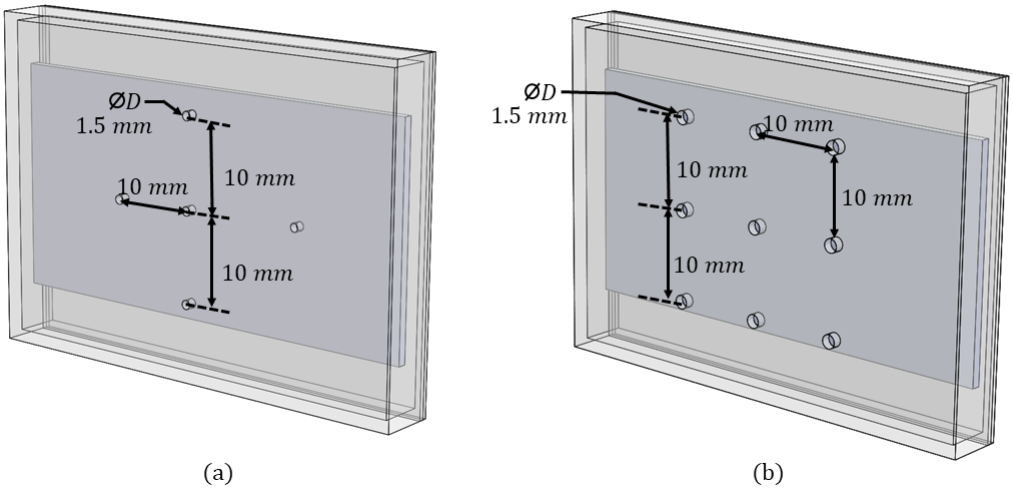

Figure 3-4: Different arrangement of nozzles. (a) Cross pattern. (b) Square pattern.

3.4 Varying Configurations of Inlet Velocities

The models in this section explores how three different configurations of inlet flow velocities at the nozzles affect the temperature of a parallel plate fin. The general

velocity configuration for the bottom, middle, and top nozzle is $(v_{bot}, v_{mid}, v_{top})$. The three different chosen velocity values are x $\frac{m}{s}$, y $\frac{m}{s}$, and z $\frac{m}{s}$, where $z > y > x > 0$. The control model is the general model, where the inlet flow velocities at the bottom, middle, and top nozzles are all y m/s. For the ascending model, the velocity configuration is (x $\frac{m}{s}$,y $\frac{m}{s}$, z $\frac{m}{s}$) which are the velocities of the bottom, middle, and top nozzles respectively. For the descending model, the velocity configuration is (z $\frac{m}{s}$, y $\frac{m}{s}$, x $\frac{m}{s}$). All the nozzle diameters are set to 1.5 mm and the impingement height is 2 mm.

3.5 Multi-jet Impingement Air Heat Exchanger

This section presents the model for the multi-jet impingement air exchanger. The model, as shown in Figure 3-5, incorporates elements from the other sections. The parallel plate fin heat sink is composed of four parallel plate fins in the general modeled spaced at 5 mm apart. The parallel manifold channels are altered from the box in the general model. Pressurized cold air enter the heat exchanger though the main inlet located at the top of the parallel manifold channels. The air first travels through the channels to jet impinge the parallel plate fins and then exit at the outlets located at the bottom of the heat exchanger. To simplify the simulation, there are two walls covering the front and back sides of the model.

Figure 3-6 is a cross section revealing the nozzles on parallel manifold channels. The nozzles are arranged in the square pattern shown in Section 3.3. The nozzle diameters are set to 1.5 mm. The impingement height is 1.0 mm. Detailed dimensions for the multi-jet impingement air exchanger are annotated on the SOLIDWORKS drawing file located in the appendix.

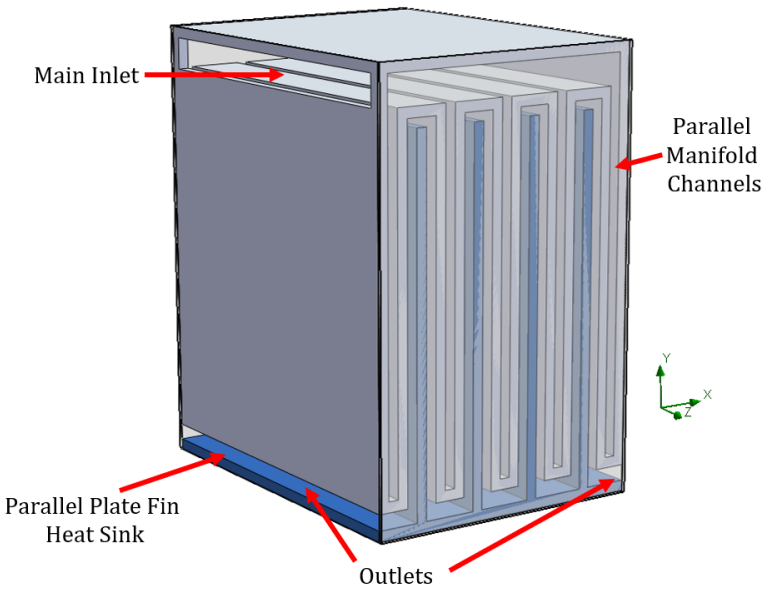

Figure 3-5: Model for multi-jet air heat exchanger.

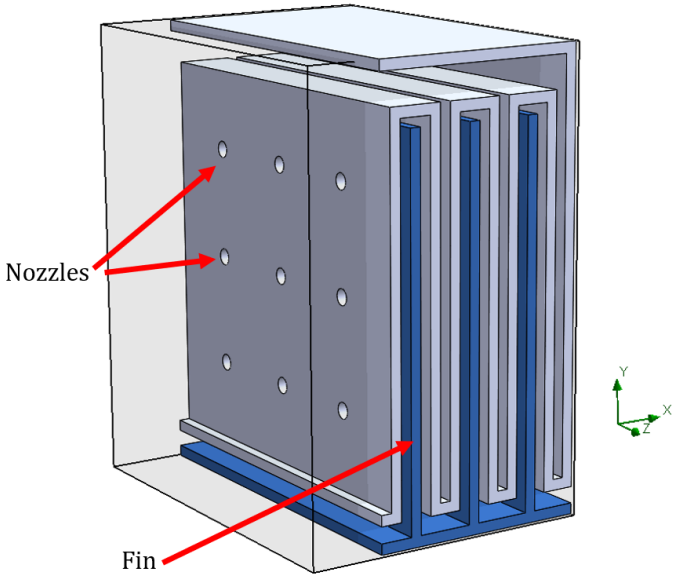

Figure 3-6: Cross section revealing the nozzles on parallel manifold channels.

Chapter 4

Method

All the models introduced in Chapter 3 were simulated using SOLIDOWORKS Flow Simulation. SOLIDWORKS Flow Simulation is a Finite Volume Method (FVM) parametric flow simulation tool used to visualize flow performance. Section 4.1 summarizes the general steps to set up the flow simulations for each model and states the assumptions for material properties and fluid volumes. Section 4.2 explains the goals set for the simulations in this paper. Section 4.3 states the boundary conditions for the models in Chapter 3.

4.1 General Steps and Assumptions

In order to perform internal flow analysis and specify flow boundary conditions in SOLIDWORKS Flow Simulation, all the model openings must be closed. Create Lids Wizard is used to create lids for nozzles in the model, as shown in Figure 4-1. Check Geometry tool is used to ensure the model is fully prepared for simulation. Internal analysis type is selected by assuming the model is enclosed. The default fluid is set to air for air jet impingement and the default solid material is set to aluminum for the fin and heat sink. The volume around the parallel plate fin is additionally selected as a fluid subdomain. No wall conditions are set, assuming the impingement walls are smooth. The model solution type is set to steady state, allowing the solution to iterate until it converges. The Result Solution Tool is responsible for mesh refinement

and analysis accuracy. It is set to resolution 3 due to limit in CPU and memory at the time this paper was written. The gap size between the exit of the nozzle and the impingement wall is specified in the Geometry Resolution tool. To add a heat source to the bottom of the fin, conduction in solid and gravity is enabled in model setup.

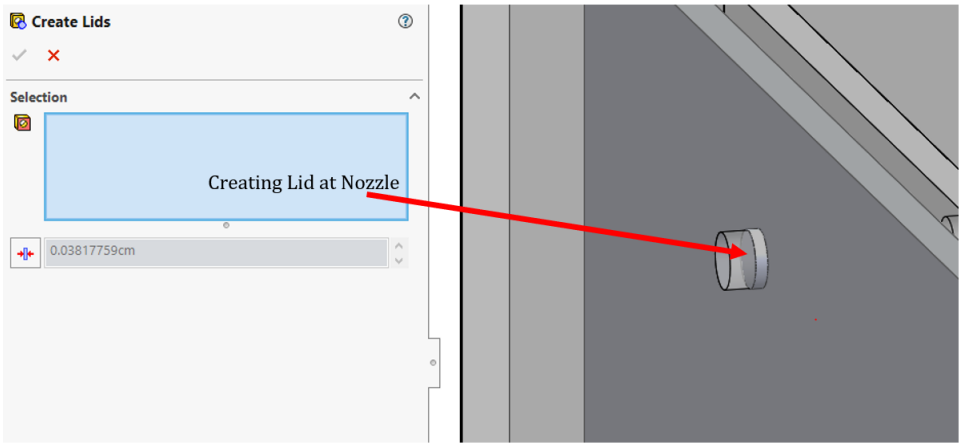

Figure 4-1: Using Create Lid Wizard to close openings. Openings must be closed to perform internal flow analysis in SOLIDWORKS Flow Simulation.

4.2 Goals

SOLIDWORKS Flow simulation allows user to set specific engineering goals and keep track of variables of interest. These goals include global goals, volume goals, surface goals, point goals, and equation goals. The goals of this paper are to track the wall temperature of the impingement surface, the solid temperature of the fin, and the temperature contour around the fin.

4.3 Boundary Conditions

For the models in Section 3.1, 3.2, and 3.3, the inlet and outlet boundary conditions and the heat source are the same. The heat source is applied at the bottom surface of the parallel plate fin. Table 4.1 lists the boundary conditions for these sections. For the models in Section 3.4, the boundary conditions are all the same with the exception of the inlet velocities. Specific values for the inlet velocities are discussed

in Chapter 5. A different set of boundary conditions were applied for the simulation of the multi-jet impingement air heat exchanger in Section 3.5. Table 4.2 lists the boundary conditions for the multi-jet impingement air heat exchanger simulation.

Parameter	Value
Inlet fluid velocity	30 m/s
Inlet fluid pressure	689,476 Pa
Inlet fluid temperature	276.15 K
Outlet fluid pressure	101,325 Pa
Outlet fluid temperature	293.2 K
Turbulence model	$\kappa - \epsilon$
κ	1 J/kg
ϵ	1 W/kg
Heat generation	10 W

Table 4.1: Boundary conditions for models in Section 3.1 - 3.4. Note that inlet velocities are different for models in Section 3.4.

Parameter	Value
Inlet fluid velocity	5 m/s
Inlet fluid pressure	689,476 Pa
Inlet fluid temperature	276.15 K
Outlet fluid pressure	101,325 Pa
Outlet fluid temperature	293.2 K
Turbulence model	$\kappa - \epsilon$
κ	1 J/kg
ϵ	1 W/kg
Heat generation	100 W

Table 4.2: Boundary conditions for the multi-jet impingement air heat exchanger.

Chapter 5

Results and Discussion

This chapter highlights simulation results for the models presented in Chapter 3. Section 5.1 presents the results for varying nozzle diameters. Section 5.2 presents the results for varying impingement heights. Section 5.3 presents the results for different arrays and patterns of nozzles. Section 5.4 presents the results for different velocity configurations. Finally, Section 5.5 presents the temperature contour and velocity trajectory results for the multi-jet impingement air heat exchanger. In summary, cooler fin temperatures occur with larger nozzle diameters, more nozzles, and lower impingement distances. Cross-flow interference are observed in the models with the cross and square pattern. Flow trajectories in simulation for the multi-jet impingement air heat exchanger reveal signs of turbulence around sharp corners and turns.

5.1 Larger Nozzle Diameter Lower Fin Temperature

The simulation results for three different nozzle diameters are presented in this section. As noted in the last chapter, the inlet and outlet boundary conditions and impingement height are the same across the three models. The three different nozzle diameters simulated are: 0.75 mm, 1.0 mm, and 1.5 mm. Figure 5-1 shows the temperature contour map from the side plane for the parallel plate fin, the air volume around the fin, and the box. Qualitatively, the model with 1.5 mm nozzles has a cooler temperature contour in comparison to the models with smaller nozzles.

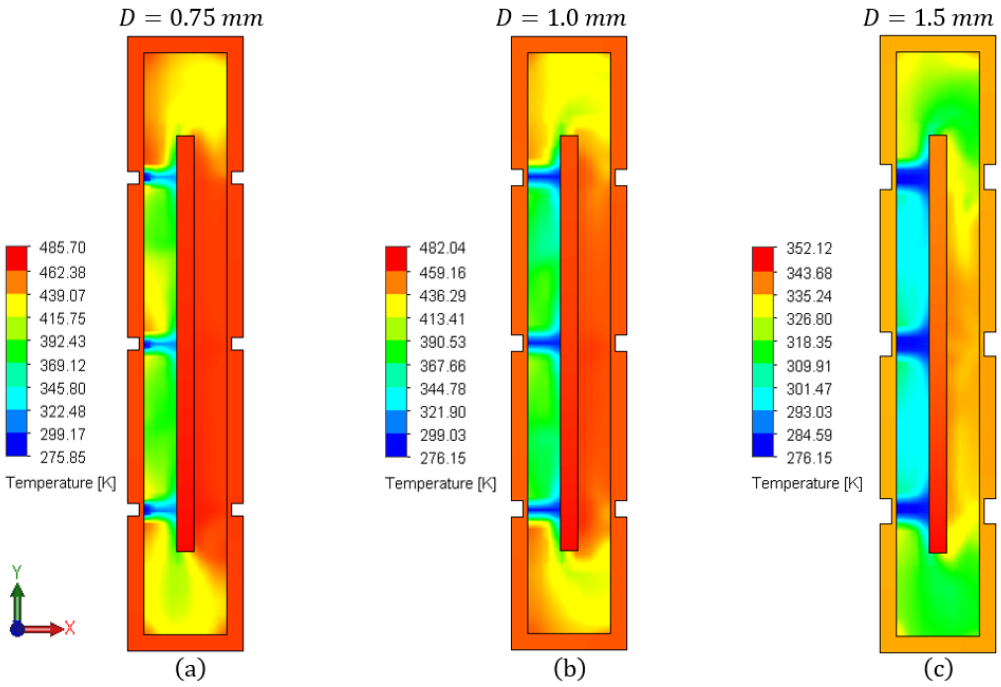

Figure 5-1: Temperature Contour Map for Different Nozzle Sizes. (a) D = 0.75 mm. (b) D = 1.0 mm. (c) D = 1.5 mm.

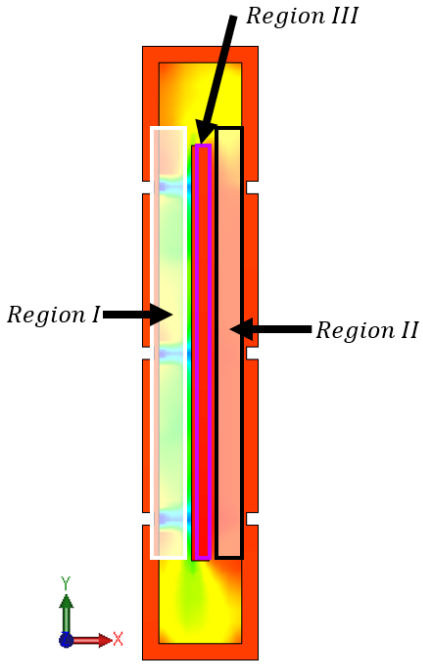

Figure 5-2: Regions with highest temperature differences.

There are three noticeable temperature differences across the three models. Figure 5-2 indicates the locations of these regions. Region I is located at the region between

the nozzles and the surface of the parallel plate fin (impingement wall). For the regions between each air jet, the temperature range is around 293.03 K and 309.91 K, which is approximately 18 to 20 percent lower than the same regions for the other two nozzle sizes. Region II is located between the fin and the outlet nozzles. The highest temperature in this area for the 1.5 mm nozzle model is approximately 342.68 K, which is approximately 110 to 140 K cooler in comparison to the same regions for the other two models. The third noticeable temperature difference is located at the surface of the fins. This can be visualized more clearly with the surface temperature plots of the parallel plate fin in Figure 5-3. These patterns make sense because as the nozzle diameters increase, heat transfer rate increases with increased surface area exposed to the air from the jet.

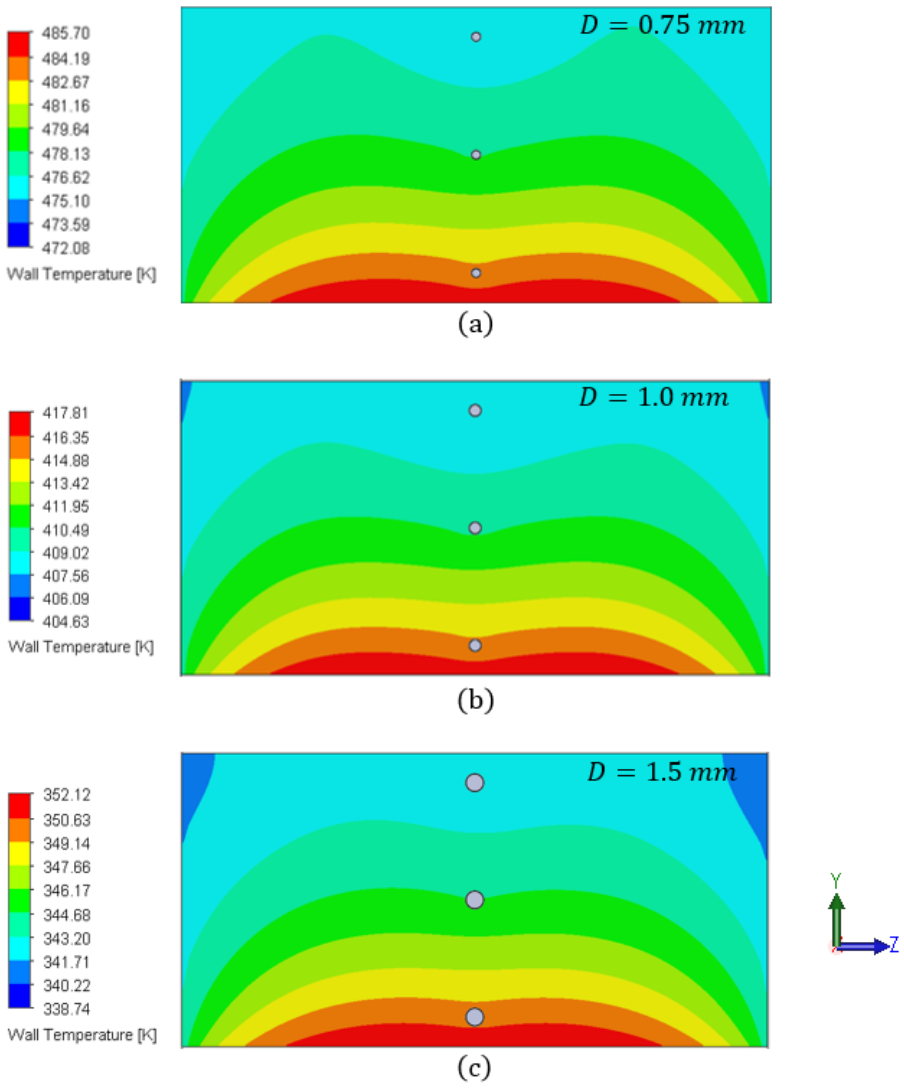

Figure 5-3: Fin surface temperature plot for different nozzle diameters. (a) D = 0.75 mm. (b) D = 1.0 mm. (c) D = 1.5 mm.

5.2 Varying Impingement Height

In this section, the model is simulated at three different impingement heights: 1.0 mm, 2.0 mm, and 3.0 mm. The inlet and outlet boundary conditions and nozzle diameter (1.0 mm) are the same across the three models. To recap, impingement height is the distance between the exit of the nozzles and the surface of the fin facing the nozzles. The same qualitative analysis strategy from Section 5.1 is applied here as well. By observing the temperature contour map from the side plane in Figure 5-4, the temperatures are warmer for the model with an impingement height of 3

mm. The maximum temperature value for this model is 482.04 K, which is almost 60 K higher than the other two models. In reference to Chapter 2, Zuckerman and Lior (2006) stated that a free jet region may not exist if the impingement height is within twice the diameter of the nozzle. The model with an impingement height of 1 mm does not satisfy this condition. The discontinuity and the blend of temperature regions between the nozzle exit and the fin surface perhaps indicate the nonexistence of a free jet region.

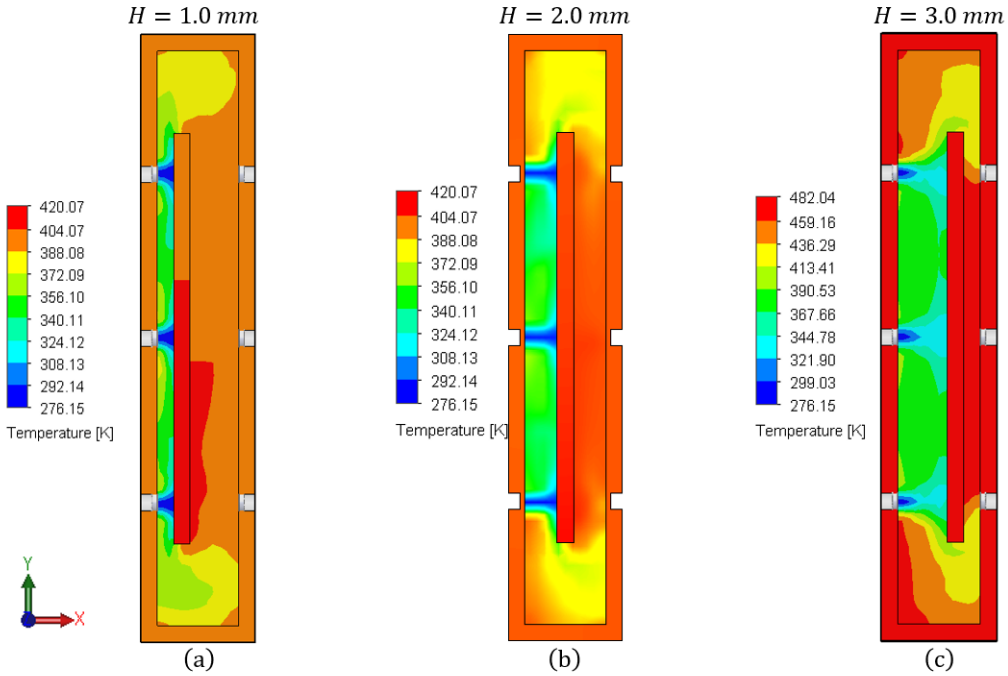

Figure 5-4: Temperature contour for varying impingement Height. (a) H =1.0 mm. (b) H = 2.0 mm. (c) H = 3.0 mm.

The surface temperature plots of the parallel plate fin in Figure 5-5 show how the temperature is changing along the fin. The discussion on temperature gradients is also reflected in this figure. The bottom of the fin is warmer due the location of the heat source. At H = 1.0 mm, the minimum temperature region on the surface of fin is significantly larger in comparison to the other models. Additional simulations are needed to confirm the accuracy of this plot.

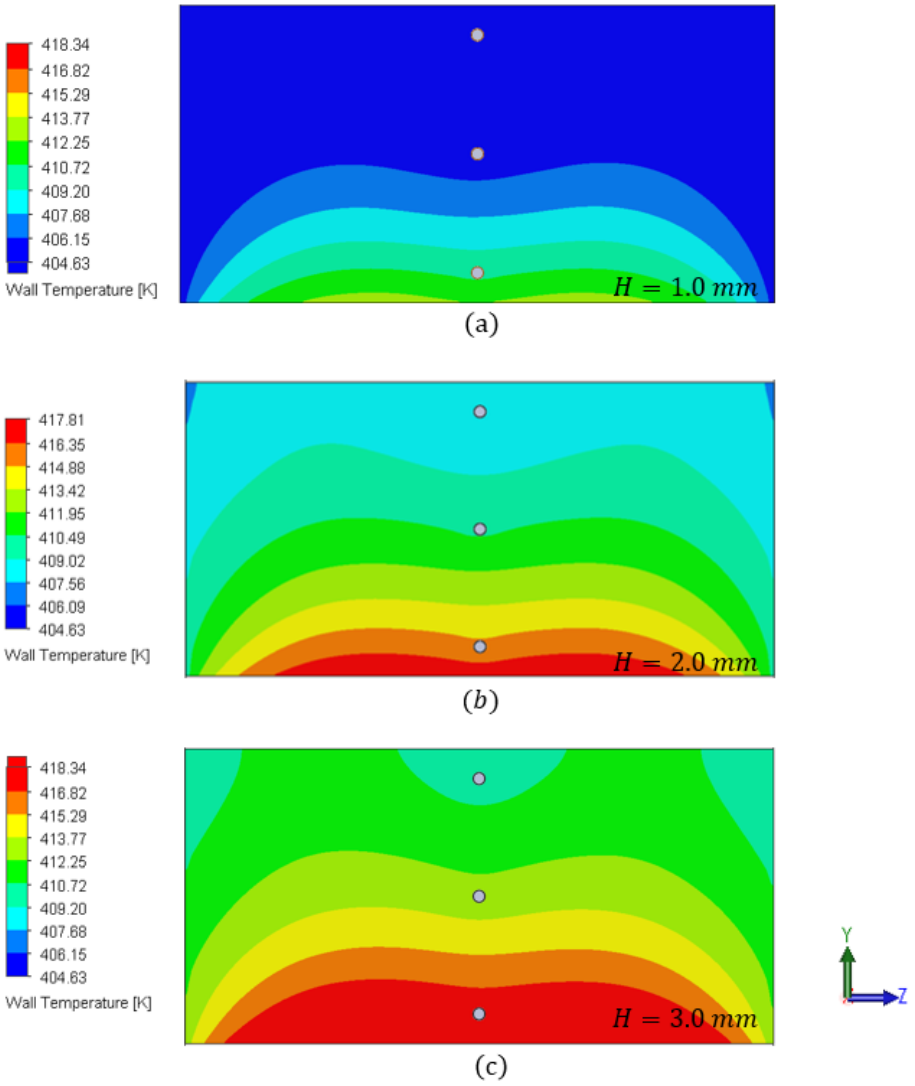

Figure 5-5: Fin surface temperature plot for different impingement heights on the Y-Z plane. (a) H =1.0 mm. (b) H = 2.0 mm. (c) H = 3.0 mm.

5.3 Nozzle Arrangement

The simulation results for three different pattern of nozzles are presented in this section. The first pattern is the general model with a single array of three nozzles along center line. The second pattern is an array of nozzles in a cross formation. The third pattern is a 3 by 3 nozzle square pattern. Illustrations of these models can be found in Chapter 3. The inlet and outlet boundary conditions, impingement height, and nozzle diameters are held constant across the three models. The impingement height is set 2.0 mm and the nozzle diameter is set to 1.5 mm. The temperature contour

plots in Figure 5-6 and the fin surface temperature plots in Figure 5-7 indicates a cooler temperature contour for the square pattern in comparison to the other two models. For example in Figure 5-7, the area of the region with minimum temperature is the largest for the square pattern.

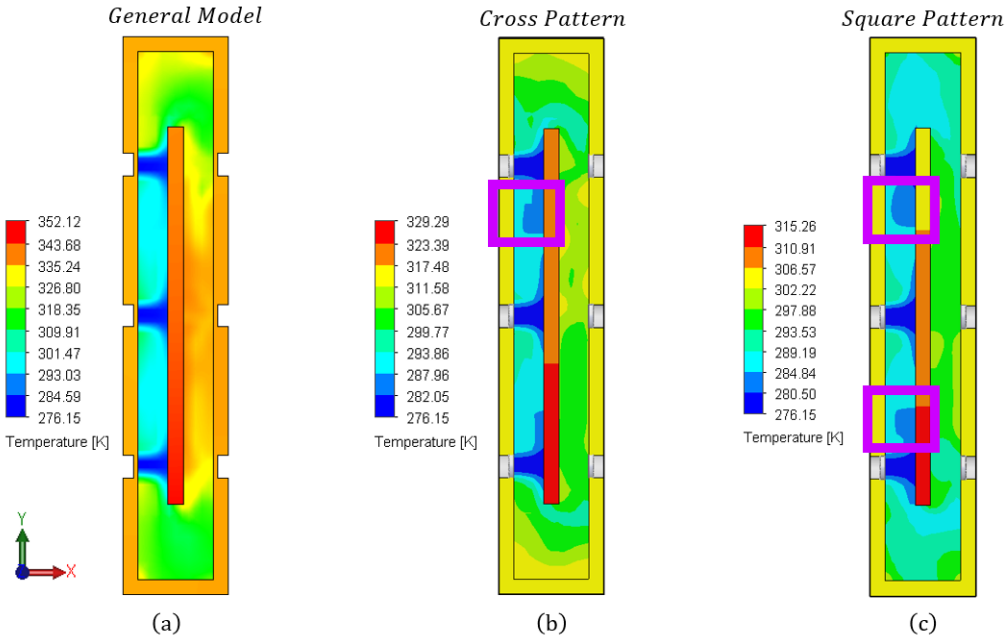

Figure 5-6: Temperature contours for different nozzle arrangements on the X-Y plane. (a) General model with single array of nozzles. (b) Cross Pattern. (c) Square pattern.

This set's results also resonate with the discussion in Section 5.1. As the number of nozzles increase, heat transfer rate increases with increased exposed surface area to the air jets. The interaction between jets creates cooler temperatures in the regions between each jet, as indicated by the purple boxes in Figure 5-6.

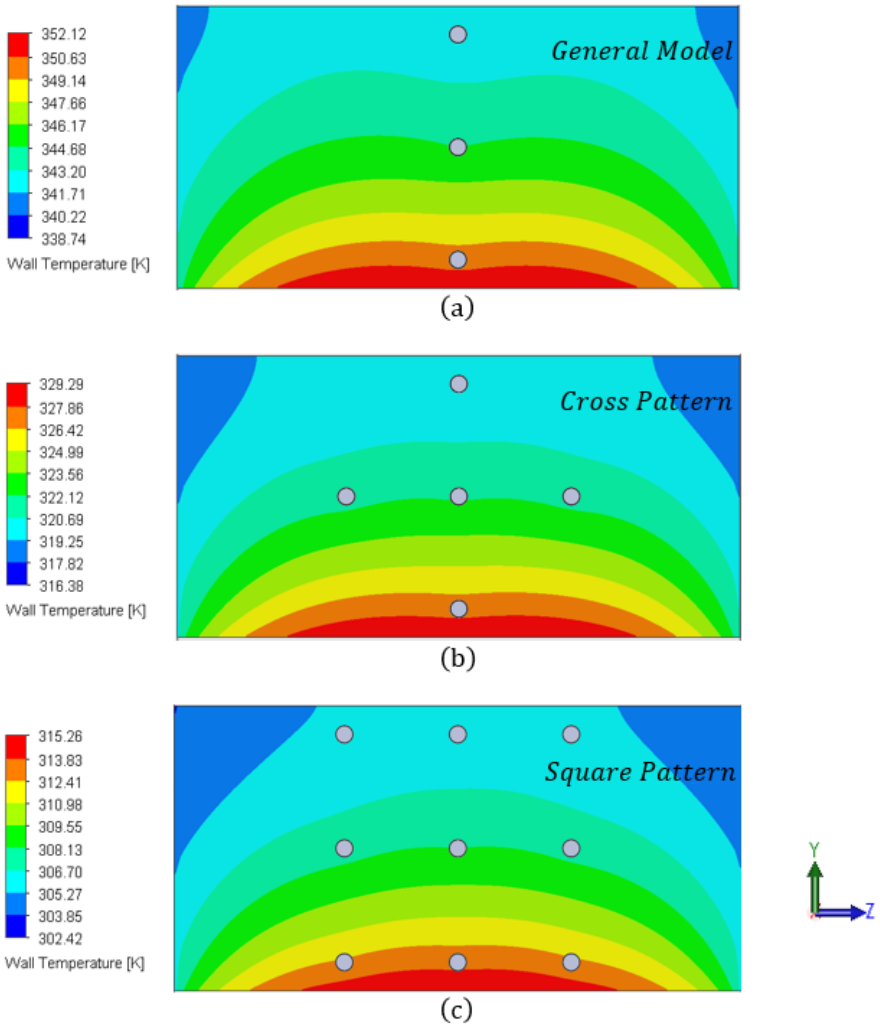

Figure 5-7: Fin temperature surface plot for different nozzle arrangements on the Y-Z plane. (a) General model with single array of nozzles. (b) Cross Pattern. (c) Square pattern.

5.4 Varying Flow Velocity at Each Nozzle

The simulations in this section explore how three different configurations of inlet flow velocities affect the temperature of the parallel plate fin. The control model is the single array model from last section, where the flow velocities at the bottom, middle, and top nozzles are all 30 m/s. For the ascending model, the bottom, middle, and top velocities are set at 30 m/s, 40 m/s, and 50 m/s respectively. For the descending model, the bottom, middle, and top velocities are set at 50 m/s, 40 m/s, and 30 m/s respectively. From Figure 5-8, the maximum temperature for all three

models is 352.12 K and the minimum temperature for all three models is 278.15 K. Although the maxima and minima are the same across the three models, the surface temperature plots for the fin surface in Figure 5-9 indicate the temperature contour for the descending model is cooler in comparison to the other two models.

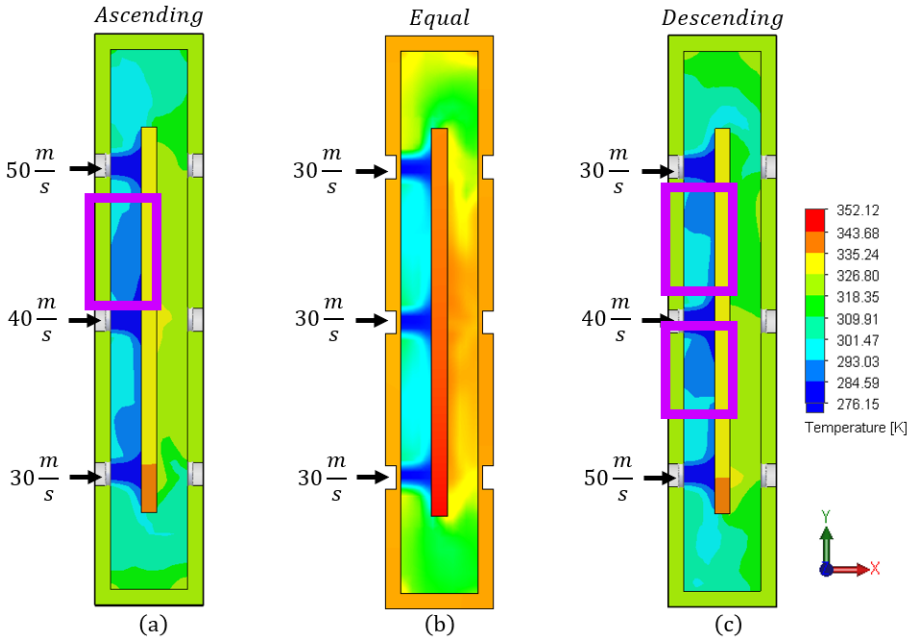

Figure 5-8: Temperature contours for different velocity configurations on X-Y plane. (a) Ascending. (b) Equal. (c) Descending.

In Figure 5-8a and Figure 5-8c, the regions indicated by the purple boxes may be mild signs of the cross flow interference. The difference in velocities across the three nozzles creates the presence of a cross flow and thickens the boundary layer. The ratio between the jet pitch and nozzle diameter is greater than 8, but the ratio between the impingement height is exactly 2. The latter case does not satisfy the spacing conditions suggested by Zuckerman and Lior (2006).

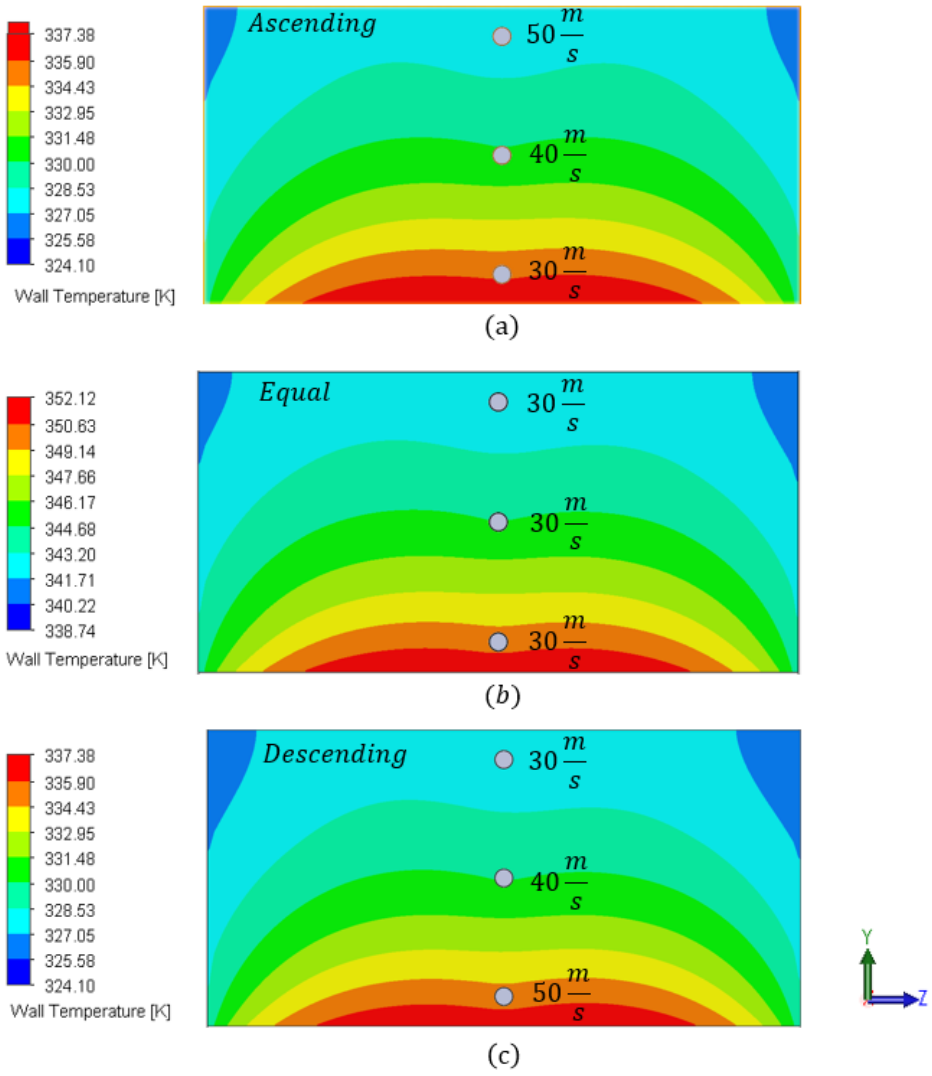

Figure 5-9: Fin temperature surface plot for different velocity configurations on Y-Z plane. (a) Ascending. (b) Equal. (c) Descending.

5.5 Multi-jet Impingement Air Exchanger

The flow trajectories for the multi-jet impingement air heat exchanger model are compared with the ideal air flow chart presented in Figure 1-2 of Chapter 1. Note that the trajectories are displayed on a plane offset from the model's X-Y plane by 20 mm. In Figure 5-10a, the nozzles are labeled from 1 to 24. Figure 5-10b and Figure 5-10c show a side by side comparison of the ideal air flow with the actual air flow in multi-jet impingement air exchanger. Ideally, there should be air flow in every single nozzle to jet impinge the fins. However, there are no air trajectories in nozzles

1 through 4 for the 100-particles simulation [1]. The red boxes in Figure 5-10c indicate the nozzles where air trajectories are present. No conclusion can be drawn about the air flow in these nozzles at the moment and using finer mesh at the nozzles may help in future simulations. Simulations reveal signs of turbulence at the top right corner of the air heat exchanger, as indicated by the purple rectangle in Figure 5-10c. This turbulence reduces air flow to the last channel on the right and is likely caused by the sharp turns at the corners of the heat exchanger. In future designs, fillets at corners should be added to reduce turbulence at these regions. An enlarged version of Figure 5-10c is shown in Figure 11. Figure 5-12 displays the solid and fluid temperature contour plots for the multi-jet impingement air exchanger model.

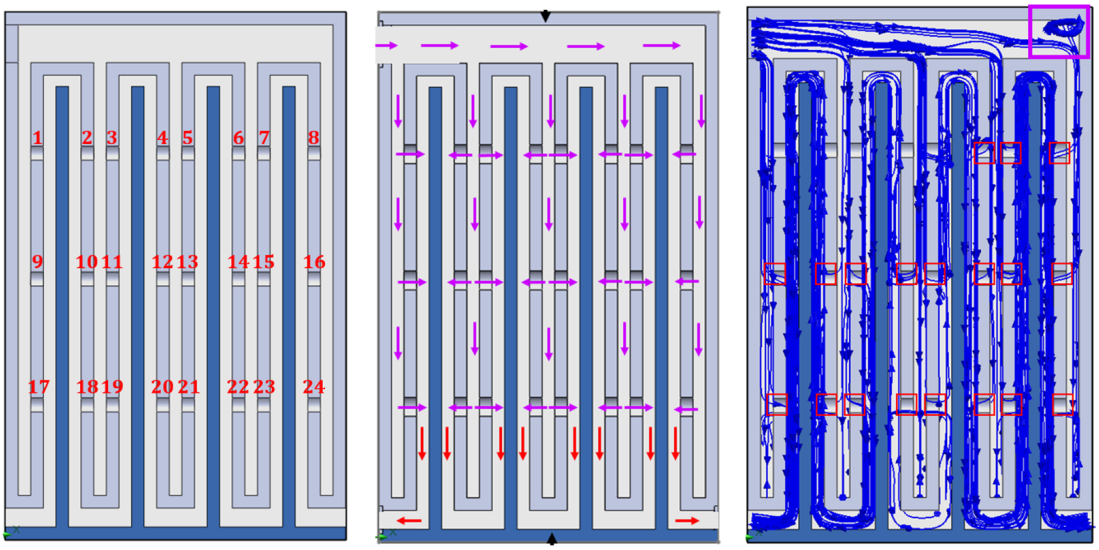

Figure 5-10: Ideal air flow vs. actual air flow in multi-jet impingement air exchanger. (a) Labels for nozzles 1 to 24. (b) Ideal air flow chart for air heat exchanger shown in Chapter 1. (c) Actual velocity trajectories inside the heat exchanger.

[1] Computer had problems loading the simulation results with more than 100 particles.

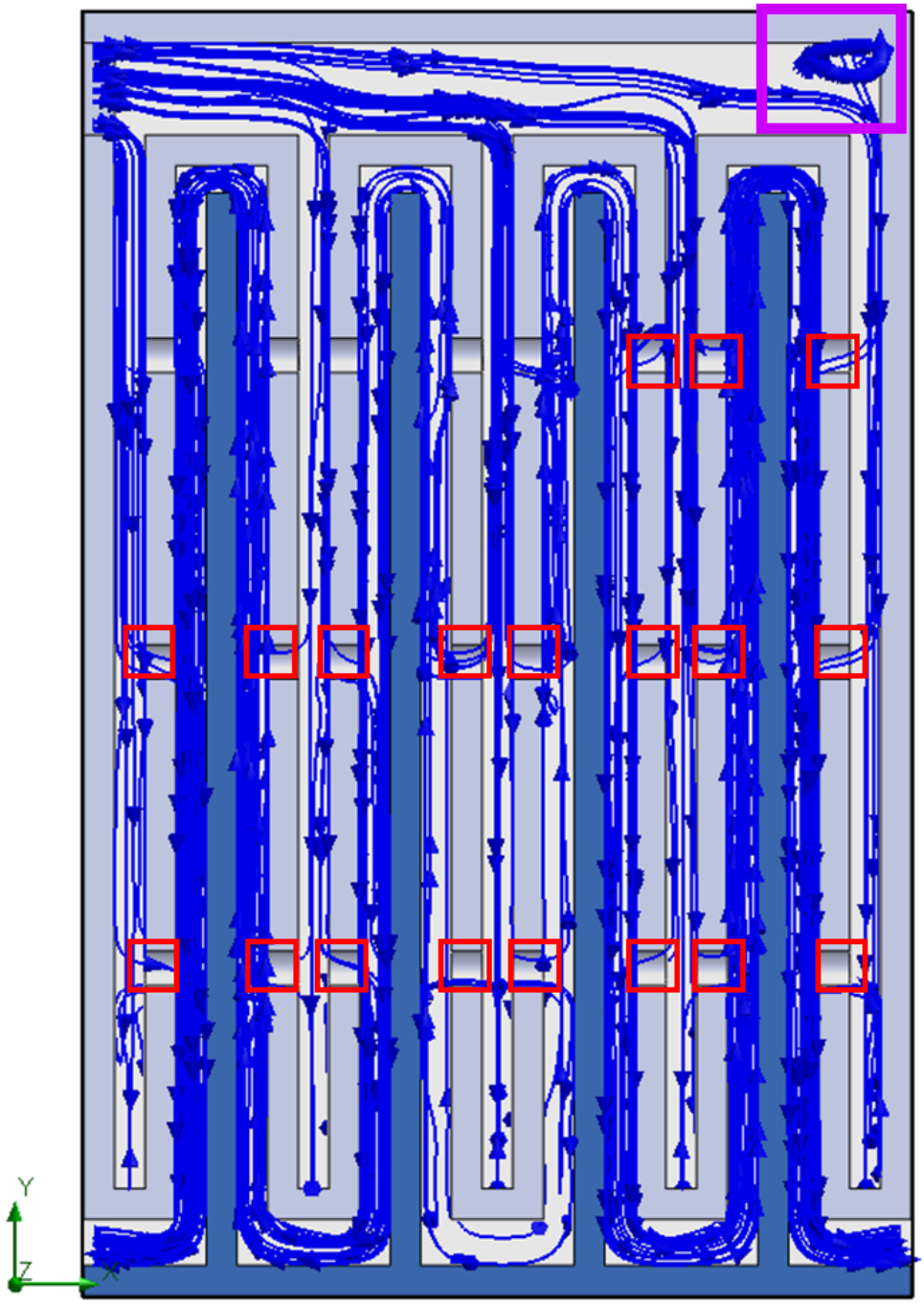

Figure 5-11: Velocity trajectories of 100 particles for the multi-jet impingement air exchanger for multi-jet impingement air exchanger. The trajectories are displayed on a plane offset from the model's X-Y plane by 20 mm.

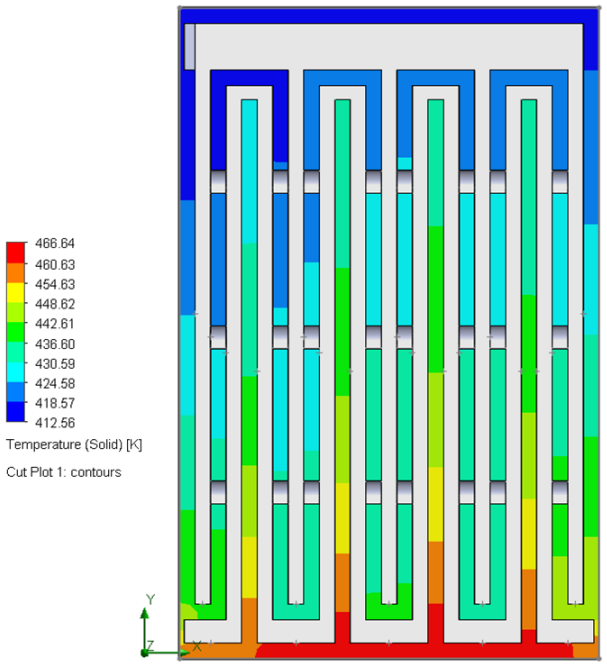

(a)

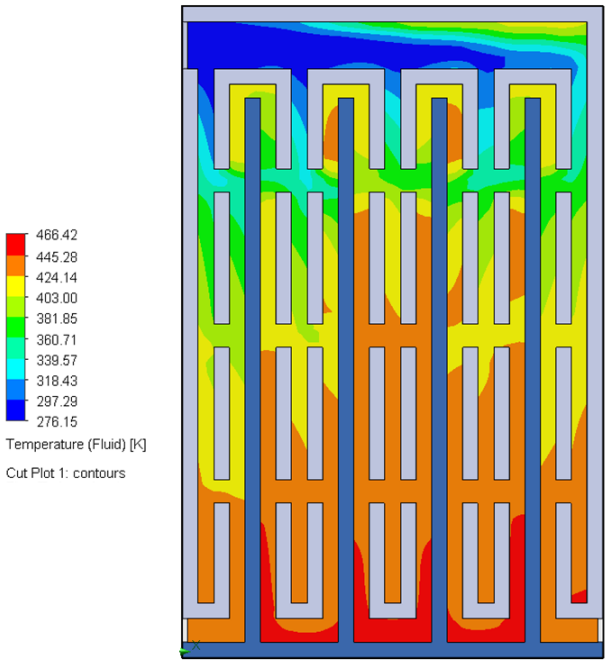

(b)

Figure 5-12: Temperature contour plot for multi-jet impingement air exchanger. (a) Temperature of the parallel plate fin heat sink and the parallel manifold channel. (b) Temperature of the air inside heat exchanger .

5.6 Conventional Parallel Flow Through Heat Sink

To compare the effects of conventional parallel flow through the heat sink with the multi-jet air impingement heat exchanger model, the parallel manifold is removed to obtain the simulation results shown in Figure 5-13. Figure 5-13a shows the temperature contour maps of the heat sink by passive cooling (heat sink only). Figure 5-13b shows the temperature contour maps of the heat sink with forced parallel air flow through the fins. The inlet velocity and the heat generation are the same as those of the multi-jet air heat exchanger model. During the simulation for the heat sink only case, the fin temperature exceeded the melting temperature of aluminum.

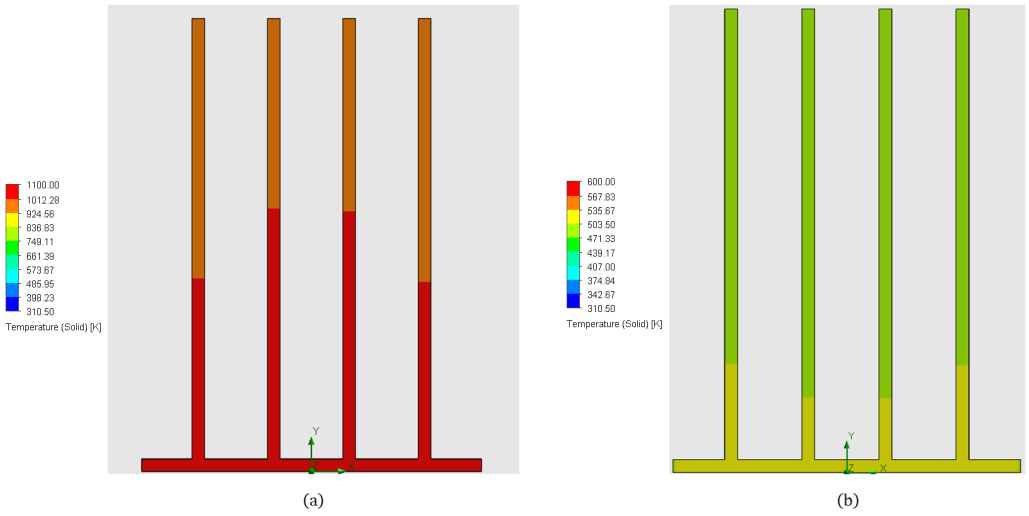

Figure 5-13: Temperature contour maps of heat sink with passive cooling and with convective cooling with heat sink. (a) Passive cooling. (b) Convective parallel air flow.

The fin thermal resistance for heat sink only case, heat sink with parallel flow case, and heat sink with the air heat exchanger is calculated in Table 5.1. The fin base temperature ($T_{fin,base}$) is approximated using the maximum temperature of the fins in the temperature contour map. The ambient temperature (T_{amb}) is approximated using the ambient temperature measured in the simulation.

Since the fins are not exposed to the ambient air in the multi-jet impingement air heat exchanger simulations, the ambient temperature is approximated by averaging the lowest and highest fluid temperatures inside the heat exchanger (445.28 K

and 318.43 K). The heat transfer rate ($\dot{Q}$) is 100 Watts as stated in the boundary conditions. The approximate fin thermal resistance is:

$$R_{fin} \approx \frac{T_{fin,base} - T_{amb}}{\dot{Q}} \tag{5.1}$$

The fin thermal resistance for the heat sink with the multi-jet air impingement is the smallest in comparison to the other two cases. Specifically, the fin thermal resistance is reduced by approximately 60 percent when compared with the fin thermal resistance of the heat sink with parallel air flow. Since the fin thermal resistance for the heat sink with the multi-jet air impingement is approximately 2.5 times smaller than the fin thermal resistance of the heat sink with parallel air flow, the heat transfer rate is approximately 2.5 times for the former case. This resonates with work by Zuckerman and Lior (2006), which stated that jet impingement has the potential to produce heat transfers rates that are three times those produced by conventional cooling methods, which confines a parallel flow to a surface.

	Heat Sink Only	Heat Sink (Parallel Flow)	Heat Sink (Heat Exchanger)
Fin Base Temperature (K)	1044.17	519.078	466.42
Ambient Temperature (K)	293.2	293.195	381.85
Fin thermal resistance (K/W)	8	2	0.8

Table 5.1: Fin thermal resistance summary.

Chapter 6

Conclusion and Future Works

The goal of the research is to analyze the design feasibility of multi-jet impingement air heat exchanger for the PEBB 6000 using SOLIDWORKS Flow Simulation. To recap, the air heat exchanger design is a two-step cooling method by combining a parallel fin heat sink and a manifold-style air heat exchanger. Different models for multi-jet impingement on a single parallel plate fin are simulated in SOLIDWORKS Flow Simulation to obtain temperature contours and flow trajectories plots. Results have shown that cooler fin temperatures were achieved with larger nozzle diameters, smaller impingement heights, higher inlet velocities, and more nozzles. These simulation designs inspired an initial model for the multi-jet impingement air heat exchanger. Compared with simulation results for the heat sink with conventional cooling by parallel air flow, the thermal resistance of the heat sink is reduced by approximately 60 percent and the heat transfer rate is 2.5 times larger with the multi-jet impingement heat exchanger setup. The sections below summarize next steps that will be taken to further understand and explore questions raised from the results in Chapter 5.

6.1 Exploring Other Parameters

To summarize, this paper explored how nozzle diameter, impingement distance, pattern of nozzles, and varying air jet velocity affect the temperature of a parallel plate fin. Some new interesting parameters to explore might include impingement wall

roughness, pulsation of air jets, jet pitch of the nozzles, and nozzle shapes. In the future, effect of wall roughness on the fin temperature could be simulated, which will provide valuable insights on selecting prototyping and manufacturing methods for the multi-jet impingement air heat exchanger. For example, due to the small size and intricate hole patterns, one possible way to build the air heat exchanger is by using Selective Laser Melting (SLM) for metal. The resulting wall roughness can be controlled by the amount of post processing.

Zuckerman and Lior (2006) mentioned that pulsed jets can result in higher or lower heat transfer coefficients due to generation of large-scale eddy currents near the exit nozzle. New simulations will be performed to evaluate the effect of pulsed air jets on the current air exchanger design. Similarly, simulations with cylindrical nozzle shapes in Chapter 5 will be alternated to include testing for other nozzle shapes. As mentioned earlier in Chapter 2, nozzle shape affects the initial conditions of the fluid exiting the nozzle. Simulation results for the model with the 3 by 3 nozzle square pattern resulted in lower temperatures on the parallel plate fin. For this model setup, the nozzle centers are equidistant from each other horizontally and vertically. It will be interesting to see how varying the jet pitch affects the temperature of fin.

6.2 Reevaluating Selected Boundary Conditions

The jet impingement simulations from Chapter 5 provide important qualitative information to how certain parameters for jet impingement affect the performance of a parallel plate fin. However, the author of this paper recognizes some of the boundary conditions selected for the simulations may be infeasible due to equipment limitations and size constraints of the air exchanger design. For example, the inlet conditions for the nozzles in the new simulations should be adjusted based on the specifications of air compressors currently available on the market. More literature review will be performed to select better and proper boundary conditions.

6.3 Optimizing Air Flow in Air Exchanger

Velocity trajectory simulation results show signs of turbulence at sharper corners, which might cause short throat and sharp heal problems and decrease the performance of the multi-jet impingement air exchanger. Some future geometric modifications to the air exchanger may include more fillets at corners. More research into the manifold design will be needed to maintain uniform air flow in the multi-jet air heat exchanger.

Appendix

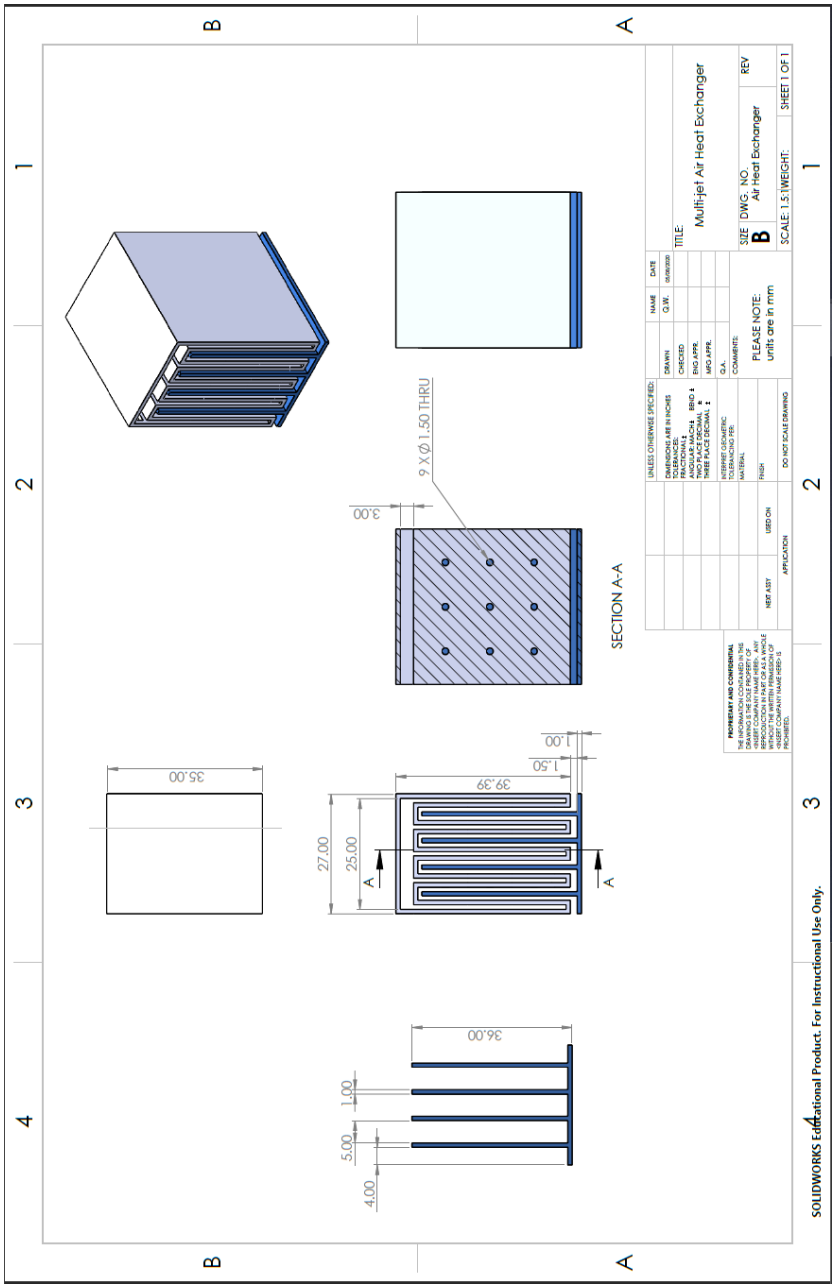
SECTION A-A
9 X Ø 1.50 THRU
3.00
35.00
27.00
25.00
39.39
1.50
1.00
36.00
5.00
1.00
4.00
Multi-jet Air Heat Exchanger
Air Heat Exchanger
PLEASE NOTE:
units are in mm
SCALE: 1.5:1
SHEET 1 OF 1
SOLIDWORKS Educational Product. For Instructional Use Only.

Bibliography

[1] Virginia Tech Center for Power Electronics Systems. Pebb 6000 thermal challenge. PowerPoint Presentation by Center for Power Electronics Systems at Virgina Tech, April 2020.

[2] John H. Lienhard IV and John H. Lienhard V. *A Heat Transfer Textbook*, chapter 4. Dover Pub., Mineola, NY, fifth edition, 2000-2019.

[3] Beomjin Kwon, Thomas Foulkes, Tianyi Yang, Nenad Miljkovic, and William P. King. Air jet impingement cooling of electronic devices using additively manufactured nozzles. *IEEE Transaction on Components, Packing, and Manufacturing Technology*, 10(2), February 2020.

[4] Electric Ship Research and Development Consortium. Thermal. PowerPoint Presentation by ESRDC on thermal management solutions for PEBB 6000, 2020.

[5] S. Yang, J.S. Chalfant, J.C. Ordonez, J.A. Khan, C. Li, I. Cvetkovic, J.V.C. Vargas, M.B. Chagas, Y. Xu, R.P. Burgos, and D. Boroyevich. Shipboard pebb cooling strategies. *2019 IEEE Electric Ship Technologies Symposium (ESTS)*, August 2019.

[6] N. Zuckerman and N.Lior. Jet impingement heat transfer: Physics, correlations, and numerical modeling. *Advances in Heat Transfer*, 39:565–631, May 2008.